Accepted for publication in *Surface and Coatings Technology*, Vol. 405, 126533, 2021, doi: https://doi.org/10.1016/j.surfcoat.2020.126533

Surface modification of AISI 8620 steel by in-situ grown TiC particle using TIG arcing

Nilesh Kumar Paraye[1], Suruj Protim Neog[1], Prakriti Kumar Ghosh[2], Sourav Das[1]

[1]Department of Metallurgical and Materials Engineering, Indian Institute of Technology Roorkee, Roorkee, PIN 247667, India

[2]Siddharth Group of Engineering Institutes, Puttur, AP, PIN 517583 India

*Corresponding author: sourav.das@mt.iitr.ac.in

Abstract:

In-situ grown titanium carbide (TiC) reinforced steel matrix was produced with tungsten inert gas (TIG) arcing by the metallurgical reaction between titanium and graphite powder on bearing steel (AISI 8620). Microstructure, chemical composition, and formation of TiC precipitate particles were thoroughly analyzed primarily for basic understanding of transformation characteristics and morphology of the TiC particles as a function of the process parameters. The microstructure was analysed with the help of several tools like field emission scanning electron microscope (FESEM) equipped with energy dispersive spectroscopy (EDS), electron probe micro analyzer (EPMA), transmission electron microscopy (TEM) and X-ray diffraction (XRD). The treated surface was practically free from cracks and porosity. The modified surface consists of in-situ synthesized titanium carbide precipitate in the martensite matrix. The XRD results confirmed the presence of titanium carbide precipitate. The changes in TIG arcing parameters have been found to vary the dilution of the modified zone which has subsequently affected the concentration of TiC precipitates in the modified region. Considerable enhancement in the mechanical properties of the modified surface was examined using microhardness and wear test. The average hardness of the modified surface with flux of lowest current reached to about 2.15 times that of the base metal. The wear test reveals the effectiveness of the TiC precipitate with the enhancement in wear resistance of about 4.6 times that of as received sample. Surface modification of the substrate was also carried out by employing TIG arcing without the addition of the flux coating to make a comparative study on the evolution of microstructure and its effect on mechanical behavior to find out the utility of using the flux coating for an exclusive benefit of the surface modification for superior properties.

Keywords: TIG arcing, surface modification, Microstructure, Microhardness, Cooling rate, Titanium carbide precipitation, wear.

Accepted for publication in *Surface and Coatings Technology*, Vol. 405, 126533, 2021, doi: https://doi.org/10.1016/j.surfcoat.2020.126533

1.Introduction

As the wear is a characteristic of surface phenomenon, its improvement is often addressed by creating a hard surface on a relatively soft substrate up to the desired depth of service demand. This approach can substantially reduce the component cost by avoiding the use of relatively costlier wear resistant material in bulk [1]. The presence of hard reinforced particles in the ductile metal matrix can render resistance to wear in abrasive applications [2]. This practice can also effectively be used to address the problem of employing general structural steel in abrasive service conditions. Further, a surface treated functionally graded composite may provide a relatively better life of the component, especially under vibrational dynamic loading, in the presence of a ductile shock absorbing back-up of bulk material. It primarily happens due to appreciable delay in on setting of premature initiation of micro cracking in the hard composite matrix or at its interface with the substrate. Thus synthesis of surface coating of particle reinforced matrix on metallic component serving in tribological applications has gathered wide attention of the technologists working in this area.

The surface composite on the metallic material has been developed by a number of researcher [3–5] using in-situ and ex-situ addition of various ceramic particles. D. sharma et al. [3] developed surface composite using ex-situ addition of SiC reinforcement which considerably enhances the surface hardness. T zhang et al. [4] synthesized the in situ grown TiB_2 reinforced metal matrix composite using Ti and AlB_2 precursor powder. Q. an et al. [5] studied the in situ formation of TiB and TiC particle which formed via the dissolution and precipitation mechanism in the Titanium alloy using TiB_2 as precursor particle. The surface composite is created by the application of various controlled heating sources including the comparatively more economical, versatile and flexibly usable tungsten inert gas (TIG) arc heating [6]. TIG arcing enables additional surface heat treatment and controlled melting of a metallic substrate in order to facilitate the modification of surface properties [7]. It is well known that the favorable condition of surface treatment of steel by employing TIG process primarily takes place owing to the development of martensitic phase in the matrix that significantly improves its wear resistance [8][9][10]. However, the desired transformation of martensite with necessary morphology to support the improved wear resistance of the substrate may not be always appreciably possible due to its strong dependence upon the chemical composition of the steel substrate. Hence, this process of surface hardening may not be significantly applicable to all kinds of steel compositions and that too especially in case of the TIG arcing as this process introduces a sharp thermal cycle of fast heating and cooling instantly at a relatively small area of arcing. In that case, introducing reinforcement particles along with hardened martensitic top layer on the steel substrate may add further versatility of TIG arcing to introduce the desired hardening of the surface to satisfy the necessary wear resistance of the material in a given service condition. Thus, by application of TIG arcing process, an in-situ creation of reinforced particles in a partially hard matrix is favored due to the possibility of introducing relatively fine particle reinforcement with practically cluster free homogeneous distribution in the matrix [8]. This is because fairly homogeneous alloying distribution in the fused matrix promotes the formation of uniformly distributed fine particles. Whereas, incorporation of ex-situ added, comparatively bigger particles and their uniform distribution by the maragoni flow of molten metal under TIG arc heating is comparatively difficult [8][9]. It is important to consider the Maragoni flow in molten substrate during arcing as a function of its parameter and melt chemistry [8,11]. This is necessary in order to create a homogeneous distribution of fine particle along the top to bottom of the fused zone allowing formation of uniformly distributed fine reinforcement. The dispersoid formed during in-situ reinforcement is thermally stable, and leads to low deterioration in service at elevated temperatures [12].

Accepted for publication in *Surface and Coatings Technology*, Vol. 405, 126533, 2021, doi: https://doi.org/10.1016/j.surfcoat.2020.126533

Various kinds of reinforcements had been used in developing a composite layer on steel substrate. Amongst these carbide reinforced metal matrix composite coatings indicates the great potential to provide good corrosion and wear resistant surface [13]. Out of various carbide ceramic particulates (e.g. TiC, SiC and WC, etc.) TiC used as reinforcement in metal matrix coating on a metallic substrate. The TiC is widely accepted as the most potential one owing to its excellent hardness, high modulus, elevated melting temperature, and very good flexural strength [13]. However the properties of in-situ formed carbide metal matrix composite coating depend on several parameters like morphology, volume, size and distribution of the reinforcement phase etc. [14]. However, their control in arc melting is not well understood so far. The extent of formation and growth in the size of in-situ developed carbide particles are largely governed by its reaction kinetics under the significantly rapid thermal cycle. The rapid cooling may cause inadequate carbide formation due to increased solubility of carbide forming elements in super saturated matrix. However, an excessive formation and growth of carbide reinforcement may reduce the toughness of surface coating and attribute to the generation of micro cracks during melt solidification with the development of residual stresses in the coating [15]. An increase in amount and decrease in size of the reinforcement are the favorable factor for wear resistance since large reinforced carbide particles are prone to develop cracks at the particle-matrix interface [16]. Thus very fine reinforced surface composite coating seems to be a good proposition for obtaining a suitable microstructure. But few researcher [17][18] have different opinion and reported that large sized carbide particles reduce the wear loss, as larger carbides are effective in supporting the load applied and preventing the metal to metal contact. The particle having angular morphology shows half of the wear rates than with the reinforcement of globular shape [16]. It was reported that higher the number of SiC particles, the more obstacles would be available for the dislocation movement and when the dislocation movement is restricted it will experience higher mechanical properties [19]. Anijdana et al. [20] reported the wear behavior of Ni-P-Cu nano-composite coatings over St37 steel and found that wear resistance of the coating was improved for higher concentration of the particle. Sabzi et al. [21] reported that increasing the amount of W_2C particle to 20% in the nanocomposite coating reduced the wear rate and coefficient of friction by 50%. The wear behavior also depends upon the matrix microstructure, according to various studies [22][23][24]. It has been argued in these studies that martensite has excellent wear resistance as compared to the different structures (ferrite, pearlite, bainite). High hardness of the martensite prevents scoring and indentation by abrasives whereas large flow stress of martensite holds the deformation bound under elastic regime as far as the contact stress do not exceeds the elastic limit [24]. It also prevents the sticking of the contact surface and prevents the adhesive wear. The wear mechanism of the martensite phase is mostly material removal in the form of micro cuttings, where it gets detached from the trenches of the worn surface [24][25].

In view of the above, an attempt has been made in this study to understand more clearly the formation and growth characteristics of in-situ developed TiC in a steel substrate during TIG arcing at different parameters on a Titanium powder and graphite containing flux coating on it. The effect of heat and thermal cycle on the formation, distribution, and morphology of TiC in the matrix were thoroughly analyzed. The effect of particle reinforcement and its distribution across the depth on the change of matrix hardness of the modified zone has been studied. Finally, the significant advantage of surface modification of the steel through reinforcement of in-situ grown TiC precipitate particle in the hardened martensite matrix on the improvement of wear resistance of the substrate is discussed.

Accepted for publication in *Surface and Coatings Technology*, Vol. 405, 126533, 2021, doi: https://doi.org/10.1016/j.surfcoat.2020.126533

2 Experimental

2.1 Material

In-situ grown TiC reinforced surface modification of bearing steel (AISI 8620) was carried out on a workpiece having a dimension of 100 mm x 65 mm with a thickness of 20 mm. The microstructure of the as received material has been shown in Fig. 1(a) which consists of proeutectoid ferrite and pearlite phase with the average grain size of 14±4 µm and 21±5 µm respectively. The fraction of ferrite and pearlite phase was in a ratio of 55:45. As a precursor, titanium powder of 99.9% purity with an average particle size of 18±9 µm and graphite powder of 27±11 µm average particle size were procured from commercial sources. Morphologies of the Ti and graphite powders can be seen in Fig. 1(b), (c). Prior to their use, the titanium and graphite powders were combined together in a ratio of 80:20 to commensurate the stoichiometry of TiC. The mix was blended in a tumbler for 3 hours in order to have a practically homogenous mixture of the powders.

Fig. 1

2.2 Preparation and modification of surface by TIG arcing

A powder mix containing about 80 and 20 wt. % of Ti and graphite powder respectively was prepared. A flux of the powder mix was prepared by adding about 20 wt. % sodium silicate (Na_2SiO_3) in it. Sodium silicate was utilized for better adhesion of the flux powder on the faying surface. Prior to TIG arcing the flat substrate surface was mechanically cleaned and washed by flashing acetone in order to make it free from rust and grease as much as possible followed by application of about 1 mm thick coating of the flux containing Ti and C on a dry surface. The thickness of around 1 mm deep flux coating was confirmed by mechanical measurement using a slot of the same depth. The amount of flux present over a surface area of 65 cm^2 was estimated at about 3.2±0.1g by weight gain technique through estimating the weight of the steel plate before and after flux coating giving rise to a distribution of flux over the surface as 50 mg/cm^2. TIG arcing was used as a heat source with the non-consumable tungsten electrode of 3 mm diameter for the fusion of the substrate surface. In order to commence relatively more amount of heat on the substrate the TIG arcing was made with direct current with electrode negative (DCEN) polarity using an ESAB MEK 44C power source, while commercial argon gas with 99.98% purity was used. Gas flow rate of 8 L/min was found suitable to avoid any appreciable blowing out of the powder prior to reaction along with shielding of the arc. The schematic diagram for the surface modification using TIG arcing with the preplaced flux coating powder has been shown in Fig. 2 (a). The arcing was implemented at varying arcing current (I) where the travel speed (S) and voltage (V) of arc were kept constant at 5 cm/min and 12 ±1 V, respectively, as shown in Table-I. TIG arcing was accomplished using an automatic travel guider with a robotic arm to keep the speed constant throughout the process. R- type thermocouple wire (Platinum-13% Rhodium) was used in order to measure the temperature profile of the fusion zone during arcing. The thermocouple tip was placed at a predetermined location from the bottom of the plate through a drill hole so that it can touch the fused zone, as it is schematically shown in Fig. 2 (b).

The selection of process parameter was made on the basis of the minimum requirement of heat input observed in an earlier work [8][9] for necessary fusion and desired reaction to form TiC at the substrate surface, where the arc travel speed was used to determine the reaction

Accepted for publication in *Surface and Coatings Technology*, Vol. 405, 126533, 2021, doi: https://doi.org/10.1016/j.surfcoat.2020.126533

time per unit length of the path of arcing. For a comparative study, surface modification of the substrate was also accomplished using the autogenous TIG arcing at the same arcing parameters with no application of flux coating. The heat input (Q) was estimated as follows [26], considering the arc efficiency (n) as 0.75.

$$Q = [(n \times I \times V \times 60)/(S \times 1000)] \quad \text{---------- (1)}$$

Fig. 2

Table-I

2.3 Microstructure

Transverse sections of the surface treated substrates, prepared by arcing with and without flux coating, were cut out utilizing an abrasive cutting machine under a water jet cooling system and prepared for metallographic characterization of microstructure. The samples were metallographically polished by sequential use of relevant grades of silicon carbide emery paper followed by fine diamond paste. Further the polished samples were etched with Nital (3.5 % HNO_3 in ethanol) solution and used as specimens for studies under different microscopes. The macro and microstructures of the specimens were initially studied under an optical microscope in order to realize the geometry of modification and micro-constituents of the matrix. The microstrusture was also studied under the field emission scanning electron microscope (FESEM) equipped with EDS detector (FEI Quanta).

2.4 Chemical analysis

The constituent elements of the steel substrate and the modified surface prepared at different arcing current with flux coating, were determined under optical emission spectroscopy and shown in Table-II. Chemistry of the constituents present in the modified surface with flux were examined using the energy dispersive spectroscopy (EDS). Elemental distribution in the surface was mapped under field emission scanning electron microscope (FESEM) with the help of an electron probe micro analyzer (EPMA) using wavelength dispersive spectroscopy (WDS). The titanium carbide precipitate formed in the modified surface was extracted by dissolving the matrix in 5% nital (5 % HNO_3 in ethanol) solution and studied by extraction replica method, where the carbon replica film was generated in the ethanol solution and directly collected on a copper grid for analysis under JEOL FE 3200FS high-resolution transmission electron microscope (HRTEM-300 kV).

Table-II

2.5 XRD analysis

To study the phase formation in the treated surface X-ray diffraction (XRD) analysis was performed by obtaining spectra from Rigaku smartlab diffractometer. The diffraction patterns were acquired within the 2θ range from 30° to 130° using Co-Kα (λ=1.79 Å) radiation at 40 kV and 30 mA. The parameter used for scanning was 0.02° of step size and rate of scanning was kept at 1°/min. The XRD analysis of phases was carried out on the modified surface that appeared as a layer on the substrate. The investigation was also performed on the precursor powder mix and base metal in order to confirm the presence of Ti and free carbon in them.

2.6 Hardness test

Hardness of the surface modified by arcing without and with flux was evaluated by measuring across the cross section using a Vickers microhardness tester operated with a load of 500 g and dwell period of 20s. The test was carried out using the ASTM E92 – 17 standard.

Accepted for publication in *Surface and Coatings Technology*, Vol. 405, 126533, 2021, doi: https://doi.org/10.1016/j.surfcoat.2020.126533

Separation between the two consecutive indentations was kept around 3-4 times the diagonal of indentation.

2.7 Wear test

Dry sliding wear tests were performed with the help of pin on disk tribometer where the specimens having modified surface with and without the additions of flux were used as pin against a standard counterbody disc of 52100 steel having 65 HRC hardness value. The tests were conducted as per ASTM G99 standard. Cylindrical pin sample of dimensions 10mm x 3mm ϕ were used. Both the disc and the pin samples were polished with 2000 grit size paper before testing. The tests were performed at ambient temperature with a constant loading of 20N for 60 minutes and the sliding speed was kept at 1m/s. Weight loss of the sample was estimated after each testing. Three samples for each condition were tested to check the repeatability of the data.

3. Results and Discussions

3.1 Evolution of microstructure

The appearance of fusion zone (FZ) followed by heat affected zone (HAZ) formed in case of arcing with and without flux coating has been typically shown in the macrographs presented in Fig. 3(a) and (b) respectively for different arcing current. The macrographs show that the depth and size of the FZ as well as the width of HAZ in base metal, appreciably increases with the increase of arcing current that enhances the heat input. The figure also shows that at a given heat input, the depth and area of FZ relatively increases with the application of flux coating. This is in agreement with the exothermic reaction of the formation of TiC during arcing with flux coating that adds extra heat to the fusion zone [27]. The typical trend of increase of depth and area of FZ and its HAZ with the increase in the amount of heat input in case of surface modification with and without utilizing flux has been shown in Table-III. It also confirms that the application of flux appreciably enhances the depth and area of FZ and its HAZ at every heat input, where the increase of it always enhances them significantly.

Fig. 3

Table-III

Fig. 4 shows the optical microstructure of the modified surface at different parameters without and with the application of flux. All the modified surface consists of martensite as a matrix phase. It can be seen that the structure becomes finer with the addition of the flux. This refinement is attributed due to the formation of titanium carbide precipitate, which hinders the grain growth by pinning action. The average grain size of the fusion zone of treated surface with flux at 80A current is reduced to 15.8 ± 4 µm as compared to the grain size of the treated surface without flux as 125 ±12 µm. Grain size of the matrix phase with the addition of flux increases with the increase in the TIG arcing current. As the current increases, the heat input also increases which leads to a slower cooling rate and hence the coarse microstructure formed.

Typical micrograph obtained from scanning electron microscope (FEG-SEM) of the modified surface prepared at different arcing currents of 80, 140 and 200 A (corresponding heat inputs can be seen in Table I) are shown in Fig. 5 (a-c) for with flux and Fig. 5 (d-f) for without flux. The microstructures presented in Fig. 5 show that the modified matrix prepared with and without flux coating at any heat input has martensite phase transformation and are

Accepted for publication in *Surface and Coatings Technology*, Vol. 405, 126533, 2021, doi: https://doi.org/10.1016/j.surfcoat.2020.126533

practically free from any flaws like pores or cracks. However, the morphology of the matrix has been changed from needle shape martensite at lower heat input to lath martensite. This might have been due to change in cooling rate for different arcing current. The change in the cooling rate can be appreciated from the thermal cycle of FZ (Fig. 6a). Associated cooling rate within 800-500ºC temperature range, denoted by t_{8-5}, and is shown in Fig. 6b which reveals a continuous decrease with increasing arcing current. During arcing on the 20 mm thick substrate the most of its portion except weld pool and HAZ remains relatively cool and behaves as a highly active heat sink reservoir, which establishes a wide temperature gradient contributing to a high rate of cooling (t_{8-5}) to the FZ. However, the characteristics of thermal cycle with respect to its cooling behavior changes significantly (Fig. 6a) with the variation of heat input where a higher heat input at larger arcing current relatively widens the width of HAZ (Table-III) that introduces a comparatively slower cooling rate (Fig. 6b) to the FZ by pushing the matrix of effective sink away from it.

The high cooling rate induces large undercooling, which further can have introduced a high nucleation rate for the precipitate [15]. The solubility of Ti and graphite in the matrix phase increases with the rapid cooling and thereby enabling Ti to remain in the form of solid solution in matrix itself [14]. The microstructures presented in Fig. 5 (a-c) also reveal the existence of well-distributed in-situ grown precipitates of TiC in predominantly martensitic matrix. The microstructures (Fig. 5 a, b and c) also show that the sizes of the in-situ grown particles vary with the arcing process parameters. It is interestingly observed that the precipitate size is relatively larger for higher arcing current of 200 A having heat input of 21.6 kJ/cm corresponding to that found in case of processing at a lower arcing current of 80 A with a heat input of 8.64 kJ/cm. In support of this observation, the measured value of variation of precipitate size with the change in TIG process parameters have been shown in Table-IV. During TIG arcing, the Ti and graphite powder are transferred from the coating to the superheated molten matrix and react to form thermodynamically stable precipitation of TiC nucleus at temperature in the range of 1500-2000°C with their subsequent growth at appropriate temperature over 900°C[28][29][30]. Higher heat input creates a wider HAZ that pushes away the colder part working as heat sink from the FZ. This can slower the cooling rate in the fusion zone and facilitates the growth of in-situ formed precipitate making them coarser. The Table-IV also shows that during TIG processing at lower heat input (8.64 kJ/cm) the fusion modified matrix is having significantly higher volume fraction (8 vol.%) of particle than that (2.1 vol.%) observed in case of processing at a higher heat input of 21.6 kJ/cm. This has happened for several reasons. Higher cooling rate induces large nucleation sites and lesser time for growth of each particles leading to a situation of many precipitate but with smaller size. However, the relative small quantity of Ti and C present in the larger FZ due to dilution effect is another reason for the reduced concentration of TiC particles in the matrix of samples exposed to higher heat input (Table-II). The increase in the current raises the heat input which melts a wider and deeper area of the base material causing a larger volume of base metal to melt. Consequently the concentration of the flux powder is reduced as compared to low current as the initial content of the flux powder was constant for all the instances. This can further reduce the amount of precipitate phase for the high heat input. The presence of the higher amount of precipitates in the FZ of relatively lower heat input has caused its appreciable grain refinement (Fig. 4 (a, b)) than those observed in case of the FZ of higher heat inputs (Fig. 4 (c), (d)) and ((e), (f)).

Fig. 4

Fig. 5

Accepted for publication in *Surface and Coatings Technology*, Vol. 405, 126533, 2021, doi: https://doi.org/10.1016/j.surfcoat.2020.126533

Fig. 6

Table IV

Typical EDS analyses of the precipitates and the matrix of the modified zone, prepared at arcing current of 80 A, are shown in Fig. 7. The Fig. 7 (a) reveals that the in-situ grown reinforced particles of the FZ are well bonded with the matrix and it contains significant amount of Ti and C (Fig. 7 (b)), whereas the matrix of FZ shows (Fig. 7 (c)) insignificant presence of Ti and C in it. It can be seen in Fig. 7(d), an EDS line scan was performed covering a line consisting of the matrix and in-situ grown precipitate and has been shown in Fig. 7 (e). It concede the existence of a significant amount of Ti in the reinforced particles present in the Fe base matrix.

In support of the above observations, the presence and distribution of *in-situ* grown TiC in the modified surface, prepared by TIG arcing at different currents of 80, 140A and 200 A, has been studied by only Ti mapping of the matrix under EPMA as depicted in Fig. 8(a), (b) and (c) respectively. All the figures show fair distribution of Ti in the matrix. The micrographs presented in the left hand side show the BSE image of the matrix. The presence of the titanium rich spots are marked with the red-colored arrow. The color code scale bar from the analytical standard used with the images, reveals the concentration of Ti at different morphological locations of the matrix. Here it is also interesting to note that the concentration of such phase is appreciably high at the grain boundary of the matrix modified at lower arcing current of 80 A (Fig. 8a) and it diminishes with the increase of arcing current to 200 A (Fig. 8c), which is in agreement to the discussions before. The observation from EPMA mapping also reveals the increase of inter precipitate distance with the increase of the arcing current, which has already been discussed earlier.

In order to reveal the type of carbide formation in the modified surface with flux, STEM imaging in HRTEM was done. Prior to imaging, the carbide layer was extracted from the modified surface as described earlier. Fig. 9 shows the STEM images of the carbide layer. It reveals the formation of the carbide on and at the vicinity of the grain boundary (Fig. 9a). Further the EDS spectrum of the particle confirms the significant presence of titanium and carbon on it, supporting the possible formation of these precipitates as TiC along the grain boundary (Fig. 9c). A different creation was chosen for conducting individual mapping of the elements, Fig. 9(d) was such area and Fig. 9(e) shows the combined elemental mapping comprising Fe, Ti and C. The presence of Fe was due to undissolved iron matrix (Fig. 9f). The individual mapping of Ti (Fig. 9g) and C (Fig. 9h) clearly demonstrate that the precipitate particles are having Ti and C as their primary elemental composition. It is worth to mention here that the precipitate particles are mostly cubical shape. This is in line with earlier studies dealt with the orientation and crystallography of TiC precipitate [31][32].

Fig. 7

Fig. 8

Fig. 9

3.2 XRD analysis

The formation of TiC precipitate in the matrix of the FZ of the surface modified substrate has been finally corroborated by the XRD investigation. The XRD analysis of the precursor powder mix and the 8620 steel substrate has been illustrated in Fig. 10 (a) and (b) respectively. The XRD graph of the precursor powder mix depicts the existence of both Ti (JCPDS 00–044–129) and C (JCPDS 00-012-0212) in it, whereas the XRD pattern (Fig. 10b) of the base metal does not show the presence of Ti in the matrix.

Fig. 10

Accepted for publication in *Surface and Coatings Technology*, Vol. 405, 126533, 2021, doi: https://doi.org/10.1016/j.surfcoat.2020.126533

Fig. 11

The diffraction pattern obtained using XRD analysis of the surface modified by TIG arcing at the different arcing current of 80, 140, and 200A has been shown in Fig. 11 (a). Further, the modified surface treated at the arcing current of 80A (Fig. 11a) shows the presence of titanium carbide precipitate in the matrix by its characteristic XRD peak (JCPDS 00-001-1222). However, compared to the total matrix, the quantity of this TiC precipitate is very small and consequently the peak intensity is also quite low. In order to establish the presence of TiC particle, the required 2θ positions are enlarged and illustrated in Fig. 11 (b) and Fig. 11 (c). The appearance of these peaks can further confirms the presence of titanium carbide precipitate in the matrix with no other significant chemical reaction of Ti in the FZ. It is worth mentioning here that the surface modified by arcing at 80A, all the three peaks of TiC from (111), (200), and (220) planes were observed at 42.1º, 49º, and 71.8º, respectively. The presence of TiC in 140A and 200A samples were not observed which could be due to the presence of even lower volume fraction (as can be seen in Table IV) as discussed above.

3.3 Hardness

Micro-hardness of the as received base material was found to be 242±7 HV. The presence of these fine reinforced particles may impart resistance to deformation and thus can exhibit significant improvement in hardness during indentation. Such behavior has been comparatively understood by studying the distribution of microhardness vertically across the modified surface from top of the FZ to base metal prepared at varying current with and without the application of flux as illustrated in Fig. 12. It shows that the hardness of the martensitic FZ without flux addition has been increased up to 466±13 HV using low arcing current of 80A which was reduced to 341±8 HV due to coarsening and auto tempering of martensite at relatively slower cooling rate of 200A arcing current (Fig. 12c). This range of hardness (~ 330-470 HV) due to martensite phase transformation in such steel with carbon content of 0.23% is in agreement to the earlier reported observations [33]. However, the average hardness observed (Fig. 12a) in the martensitic FZ of the substrate modified with flux by arcing at 80A was of the order of 533±32 HV, which was reduced to 494±22 HV (Fig. 12c) while using arcing at 200A at relatively higher heat input. Such an increment in the hardness of the treated surface with the addition of flux coating can largely be pertained to the formation of the in-situ grown titanium carbide precipitate in the martensitic matrix over that observed in the matrix with martensite transformation without having TiC particles. The maximum rise of hardness due to TiC reinforcement in the modified matrix of relatively lower heat input was found to be about 2.15 times more than that of the as received material. However, the comparatively lower hardness observed in the FZ modified at higher heat input can primarily be associated to the presence of comparatively less amount of TiC particles (Table-IV).

The micro-hardness distribution across the depth shows that the high hardness of FZ falls sharply before it reaches the steady zone of comparatively softer base metal. The characteristics of hardness distribution clearly mark the extent of the FZ and HAZ in the case of both the processes of surface modification with and without flux coating carried out at different arcing current as shown in Fig. 12. The figures reveal that with the increment in heat input due to the increase of current always relatively enhances the depth of the FZ and HAZ. It is noticed that with the rise in current from 80 to 140 and 200 A, the depth of FZ enhances from 1.3 to 2.45 and 3.05 mm respectively when no flux coating is used. However, during flux coating, a relatively higher depth of FZ, (1.45 to 2.6 and 3.9 mm for 80, 140 and 200A respectively) has been noted. (Fig. 12). It may also be noted that the width of HAZ is marginally higher in case of utilizing the flux than that observed during arcing without coating. These

Accepted for publication in *Surface and Coatings Technology*, Vol. 405, 126533, 2021, doi: https://doi.org/10.1016/j.surfcoat.2020.126533

observations are closely in agreement to the observations given in Table-III and also appropriately in agreement to the discussions given above regarding the increase of heat input with the arcing current and excess heat generation due to exothermic reaction in case of utilizing the flux coating. All such behaviors of the consequence of heat input on distribution of hardness across the surface modified matrix are comparatively more prominently visible in case of using the lower and higher arcing currents of 80 and 200A, respectively.

Fig.12

3.4 Wear characteristics

The wear characteristics as a function of weight loss for a given period of testing for the as received material (8620 steel substrate) and its modified surface with and without the reinforcement of TiC precipitate produced by TIG arcing has been illustrated in Fig. 13. The surface modified by in-situ grown TiC precipitates particles, has been found to enhance the wear resistance considerably. The observed enhancement of wear resistance of the TiC particle reinforced matrix is of the order of more than four times compared to that of the as-received material. It is noteworthy that similar observation was made in earlier studies where the hardfacing was performed by using a high-energy electron-beam irradiation process [34].

The worn surfaces for the as received, with and without reinforced particles are shown in Fig. 14. From the worn surface of the as-received material (Fig. 14 (a), (d)), it can be seen that there was significant material removal through severe plastic deformation. The alternative grooves or the scratch marks in the direction of wear signify that abrasion was the primary mechanism of wear. Those abrasion marks, along with minor pits were believed to be formed as a result of the abrasive action by the hard asperities of the counterface or the wear debris on a relatively softer substrate [35]. However the presence of rough worn surface including craters and pits shows the possible presence of adhesive wear mode also [36]. On the other hand, the surface modified without flux showed a significantly lower number of grooves with small pits and crater (Fig. 14 b, e). From the SEM images it can be seen that in this case the grooves formed were relatively narrower and shallower as compared to the as received material. In this case, the wear resistance appears to be higher than the substrate material owing to the formation of a hard martensite phase. For the sample modified with flux, a very few scratch marks with a relatively smoother surface as compared to the other two conditions was observed as can be seen in Fig. 14 c and f. The presence of scratch marks shows evidence of abrasive mode [34,37,38]. This set of micrograph shows minimal wear which can be mainly due to the formation of carbide in the martensite matrix that might have significantly reduced the extent of abrasion by hard asperities. Formation of TiC particles in the metal matrix effectively decreases the true surface area in contact between the coated surface and the counterpart. Consequently, the final wear rate is reduced to a great extent [36][39]. The Soft matrix is prone to wear out in case of hard carbide with soft matrix leading to spalling of particles [32]. However, the spalled- out titanium carbide was also not seen in the micrographs. It indicates that the martensite matrix could strongly holds the hard, in situ formed titanium carbide which had played a crucial role in the wear resistance [32].

Fig. 13

Fig. 14

Accepted for publication in *Surface and Coatings Technology*, Vol. 405, 126533, 2021, doi: https://doi.org/10.1016/j.surfcoat.2020.126533

4. Conclusion-

A thorough study of TIG arcing on a steel substrate was conducted in order to develop a hard facing layer by in-situ precipitation of TiC particles. Several microstructural characterization were conducted to comprehend the presence, size and distribution of such particles. The following conclusions are made.

1. It can be understood that TIG arcing (TIGA) on a Ti and graphite containing coating applied on AISI 8620 bearing steel can be quite effective to modify the surface of the substrate by reinforcement of in-situ grown TiC precipitate in it.
2. The microscopic studies supported by EDS mapping, EPMA, and XRD studies appropriately established that the precipitates are of cubical shape TiC of an average size of around 0.46 µm at an arcing current of 80A.
3. Relative amount of TiC precipitate in the FZ varies with the arcing current affecting the heat input, being favored of having a larger quantity in case of using lower current of about 80 A than that occurs at higher current of 200 A due to noteworthy increase of dilution together with the reduction in the ratio between the flux material to the fusion zone.
4. Due to the presence of precipitate and the martensite matrix, the microhardness of the surface composite improved significantly from 242 HV (base) to 522, 491, and 484 HV for the sample processed with 80A, 140A, and 200A respectively.
5. The most effective TIGA processing at low arcing current of 80 A with respect to maximum increase of surface hardness, the wear resistance of the modified substrate with reinforcement is enhanced up to about 1.75 times than that of the non-reinforced modified substrate and 4.6 times than that of the non-treated base substrate.

References:

[1] B. Du, Z. Zou, X. Wang, S. Qu, Laser cladding of in situ TiB 2 / Fe composite coating on steel, Appl. Surf. Sci. 254 (2008) 6489–6494. https://doi.org/10.1016/j.apsusc.2008.04.051.

[2] A.A. Voevodin, J.S. Zabinski, Nanocomposite and nanostructured tribological materials for space applications, Compos. Sci. Technol. 65 (2005) 741–748.

https://doi.org/10.1016/j.compscitech.2004.10.008.

[3] D. Sharma, P.K. Ghosh, R. Anant, S. Kumar, Surface modification of microalloyed steel by silicon carbide reinforcement using tungsten inert gas arcing Surface modification of microalloyed steel by silicon carbide reinforcement using tungsten inert gas arcing, Mater. Res. Express. 6 (2019) 1–8. https://doi.org/10.1088/2053-1591/aaf7d8.

[4] T. Zhang, K. Feng, Z. Li, H. Kokawa, Effects of in-situ synthesized TiB 2 on crystallographic orientation , grain size and nanohardness of AA6061 alloy by laser surface alloying, Mater. Lett. 253 (2019) 213–217. https://doi.org/10.1016/j.matlet.2019.06.075.

[5] Q. An, L. Huang, Y. Jiao, Y. Bao, B. Zhong, L. Geng, Intergrowth microstructure and superior wear resistance of (TiB + TiC)/ Ti64 hybrid coatings by gas tungsten arc cladding, Mater. Des. 162 (2019) 34–44. https://doi.org/10.1016/j.matdes.2018.11.039.

[6] T.N. Baker, P.M. Escalona, M. Olasolo, J. Kelly, B. Wei, K. He, S. Mridha, T. Neville, P.M. Escalona, M. Olasolo, Role of preplaced silicon on a TIG processed SiC incorporated microalloyed steel steel, Mater. Sci. Technol. 36 (2020) 1349–1363. https://doi.org/10.1080/02670836.2020.1781355.

[7] N.K. Paraye, P.K. Ghosh, S. Das, Surface modification via in situ formation of titanium carbide in ferrous matrix through TIG arcing, Mater. Lett. (2020) 128723. https://doi.org/10.1016/j.matlet.2020.128723.

[8] D. Sharma, P.K. Ghosh, S. Kumar, S. Das, R. Anant, Surface hardening by in-situ grown composite layer on microalloyed steel employing TIG arcing process, Surf. Coat. Technol. 352 (2018) 144–158. https://doi.org/10.1016/j.surfcoat.2018.08.009.

[9] D. Sharma, P.K. Ghosh, N. Kumar, R. Anant, Surface hardening characteristics of microalloyed steel during ex-situ and in- situ Al 2 O 3 reinforcement under TIG arcing, Surf. Coat. Technol. 380 (2019) 125002. https://doi.org/10.1016/j.surfcoat.2019.125002.

[10] N.K. Paraye, P.K. Ghosh, S. Das, A novel approach to synthesize surface composite by in-situ grown VC reinforcement in steel matrix via TIG arcing, Surf. Coatings Technol. 399 (2020). https://doi.org/10.1016/j.matdes.2019.108334.

[11] E. Ahmadi, A.R. Ebrahimi, Welding of 316L Austenitic Stainless Steel with Activated Tungsten Inert Gas Process, J. Mater. Eng. Perform. 24 (2015) 1065–1071. https://doi.org/10.1007/s11665-014-1336-6.

[12] J. Li, H. Li, M. Wang, S. Wang, Q. Ji, M. Li, J. Chi, Applications of WC-based composites rapid synthesized by consumable electrode in-situ metallurgy to cutting pick, Int. J. Refract. Met. Hard Mater. 35 (2012) 132–137. https://doi.org/10.1016/j.ijrmhm.2012.05.005.

[13] S. Yang, W. Liu, M. Zhong, Z. Wang, TiC reinforced composite coating produced by powder feeding laser cladding, Mater. Lett. 58 (2004) 2958–2962. https://doi.org/10.1016/j.matlet.2004.03.051.

[14] Y. Cao, H. Ren, C. Hu, Q. Meng, Q. Liu, In-situ formation behavior of NbC-reinforced Fe-based laser cladding coatings, Mater. Lett. 147 (2015) 61–63. https://doi.org/10.1016/j.matlet.2015.02.026.

[15] B. Du, S.R. Paital, N.B. Dahotre, Synthesis of TiB 2 – TiC / Fe nano-composite coating by laser surface engineering, Opt. Laser Technol. 45 (2013) 647–653. https://doi.org/10.1016/j.optlastec.2012.05.017.

[16] K. Van Acker, D. Vanhoyweghen, R. Persoons, J. Vangrunderbeek, Influence of tungsten carbide particle size and distribution on the wear resistance of laser clad WC / Ni coatings, Wear. 258 (2005) 194–202. https://doi.org/10.1016/j.wear.2004.09.041.

[17] J.Y. Yun, G.S. Shin, D. Il Kim, H.S. Lee, W.S. Kang, S.J. Kim, Effect of carbide size

and spacing on the fretting wear behavior of Inconel 690 SG tube mated with SUS 409, Wear. 338–339 (2015) 252–257. https://doi.org/10.1016/j.wear.2015.06.012.

[18] A.T. Alpas, J. Zhang, Effect of Microstructure (Particulate Size and Volume Fraction) and Counterface Material on the Sliding Wear Resistance of Particulate-Reinforced Aluminum Matrix Composites, Metall. Mater. Trans. A. 25A (1994) 969–983. https://doi.org/10.1007/BF02652272.

[19] S.H.M. Anijdan, M. Sabzi, The effect of pouring temperature and surface angle of vortex casting on microstructural changes and mechanical properties of 7050Al-3 wt % SiC composite, Mater. Sci. Eng. A. 737 (2018) 230–235. https://doi.org/10.1016/j.msea.2018.09.057.

[20] S.H.M. Anijdan, M. Sabzi, M.R. Zadeh, M. Farzam, The influence of pH , rotating speed and Cu content reinforcement nano- particles on wear / corrosion response of Ni-P-Cu nano-composite coatings, Tribiology Int. 127 (2018) 108–121. https://doi.org/10.1016/j.triboint.2018.05.040.

[21] M. Sabzi, S.M. Dezfuli, M. Far, Deposition of Ni-tungsten carbide nanocomposite coating by TIG welding: Characterization and control of microstructure and wear/corrosion responses, Ceram. Int. 44 (2018) 22816–22829. https://doi.org/10.1016/j.ceramint.2018.09.073.

[22] S.M. Shariff, T.K. Pal, G. Padmanabham, S. V Joshi, S.M. Shariff, T.K. Pal, G. Padmanabham, S. V Joshi, Sliding wear behaviour of laser surface modified pearlitic rail steel, Surf. Eng. ISSN. 26 (2013) 199–208. https://doi.org/10.1179/174329409X455458.

[23] J. Suchánek, V. Kuklík, Influence of heat and thermochemical treatment on abrasion resistance of structural and tool steels, Wear. 267 (2009) 2100–2108. https://doi.org/10.1016/j.wear.2009.08.003.

[24] S. Das Bakshi, D. Sinha, S.G. Chowdhury, V. V Mahashabde, Surface and sub-surface damage of 0 . 20 wt % C-martensite during three- body abrasion, Wear. 394–395 (2017) 217–227. https://doi.org/10.1016/j.wear.2017.07.004.

[25] S. Das Bakshi, P.H. Shipway, H.K.D.H. Bhadeshia, Three-body abrasive wear of fi ne pearlite , nanostructured bainite and martensite, Wear. 308 (2013) 46–53. https://doi.org/10.1016/j.wear.2013.09.008.

[26] S. Kumar, P.K. Ghosh, R. Kumar, Surface modification of AISI 4340 steel by multi-pass TIG arcing process, J. Mater. Process. Technol. 249 (2017) 394–406. https://doi.org/10.1016/j.jmatprotec.2017.06.035.

[27] Naminosuke Kubota, Ti-C Pyrolants, in: Propellants Explos. Thermochem. Asp. Combust., Wiley, 2015: pp. 341–342. https://doi.org/10.1002/9783527693481.

[28] G. Zhu, W. Wang, R. Wang, C. Zhao, W. Pan, Formation Mechanism of Spherical TiC in Ni-Ti-C System during Combustion Synthesis, Materials (Basel). 10 (2017) 1–8. https://doi.org/10.3390/ma10091007.

[29] C. Benoit, H. Ellen, K. Nikhil, V. Dominique, D. Sylvain, TiC nucleation / growth processes during SHS reactions, Powder Technol. 157 (2005) 92–99. https://doi.org/10.1016/j.powtec.2005.05.035.

[30] Y.F. Yang, S.B. Jin, Q.C. Jiang, Effect of reactant C/Ti ratio on the stoichiometry, morphology of TiCx and mechanical properties of TiCx–Ni composite, CrystEngComm. 15 (2013) 852–855. https://doi.org/10.1039/c2ce26767e.

[31] J. Nie, Y. Wu, P. Li, H. Li, X. Liu, Morphological evolution of TiC from octahedron to cube induced by elemental, CrystEngComm. 14 (2012) 2213–2221. https://doi.org/10.1039/c1ce06205k.

[32] E. Yun, Y.C. Kim, S. Lee, N.J. Kim, Correlation of Microstructure with Hardness and Wear Resistance in (TiC , SiC)/ Stainless Steel Surface Composites Fabricated by

Accepted for publication in *Surface and Coatings Technology*, Vol. 405, 126533, 2021, doi: https://doi.org/10.1016/j.surfcoat.2020.126533

High-Energy Electron-Beam Irradiation, Metall. Mater. Trans. A. 35 (2004) 1029–1038. https://doi.org/10.1007/s11661-004-1006-7.

[33] I. Manna, J.D. Majumdar, B.R. Chandra, S. Nayak, N.B. Dahotre, Laser surface cladding of Fe – B – C , Fe – B – Si and Fe – BC – Si – Al – C on plain carbon steel, Surf. Coat. Technol. 201 (2006) 434–440. https://doi.org/10.1016/j.surfcoat.2005.11.138.

[34] D. Nam, K. Lee, S. Lee, Correlation of microstructure with hardness and wear resistance of carbide-reinforced ferrous surface composites fabricated by high-energy electron-beam irradiation, Metall. Mater. Trans. A. 39 (2008) 2626–2634. https://doi.org/10.1007/s11661-008-9641-z.

[35] S. P. Neog, S. Das, S. Das, Microstructural evolution of novel continuously cooled carbide free bainitic steel during sliding wear, Wear. 456–457 (2020) 203359. https://doi.org/10.1016/j.wear.2020.203359.

[36] M. Sabzi, S.M. Dezfuli, S.M. Mirsaeidghazi, The effect of pulse-reverse electroplating bath temperature on the wear/corrosion response of Ni-Co/tungsten carbide nanocomposite coating during layer deposition, Ceram. Int. 44 (2018) 19492–19504. https://doi.org/10.1016/j.ceramint.2018.07.189.

[37] J.D. Majumdar, Development of in-situ composite surface on mild steel by laser surface alloying with silicon and its remelting, Surf. Coat. Technol. 205 (2010) 1820–1825. https://doi.org/10.1016/j.surfcoat.2010.07.114.

[38] M. Sabzi, S.M. Dezfuli, Z. Balak, Crystalline texture evolution, control of the tribocorrosion behavior, and significant enhancement of the abrasion properties of a Ni − P nanocomposite coating enhanced by zirconia nanoparticles, Int. J. Miner. Metall. Mater. 26 (2019) 1020–1030. https://doi.org/10.1007/s12613-019-1805-x.

[39] S. Mersagh, M. Sabzi, Effect of yttria and benzotriazole doping on wear/corrosion responses of alumina-based nanostructured film, Ceram. Int. 44 (2018) 20245–20258. https://doi.org/10.1016/j.ceramint.2018.07.313.

Accepted for publication in *Surface and Coatings Technology*, Vol. 405, 126533, 2021, doi: https://doi.org/10.1016/j.surfcoat.2020.126533

Table-I: TIG process parameter

S.No	Sample Designation	Arcing Current(A)	Arc Voltage (V)	Arc Travel Speed(cm/min)	Heat Input (kJ/cm)
1.	M80/5	80	12	5	8.64
2.	M140/5	140	12	5	15.12
3.	M200/5	200	12	5	21.6

Table- II: Chemical composition (wt. %) of the base metal (AISI 8620 steel) and modified matrix prepared with flux coating at different arcing current.

Sample	C	Cr	Ni	Mn	Si	Mo	Al	Ti	S	P	Cu	Fe
Base	0.21	0.63	0.43	0.98	0.41	0.25	0.02	-	0.002	0.01	0.02	Rest
M80/5	0.98	0.67	0.48	0.92	0.43	0.22	0.02	7.1	0.002	0.01	0.02	Rest
M140/5	0.76	0.69	0.39	0.89	0.47	0.29	0.02	4.3	0.002	0.01	0.02	Rest
M200/5	0.41	0.65	0.42	0.97	0.38	0.23	0.02	1.9	0.002	0.01	0.02	Rest

Table-III: Depth and area of fusion zone and its HAZ in case of surface modification with and without flux.

Sample	Depth of FZ (mm)		Area of FZ (mm^2)		Width of HAZ (mm)	
	with flux	without flux	with flux	without flux	with flux	without flux
M80/5	1.41	1.3	3.74	3.7	1.4	1.0
M140/5	2.61	2.5	10.05	9.64	1.88	1.72
M200/5	3.98	3.05	21.18	18.53	2.47	2.68

Table IV: Average size and volume fraction of precipitate in the matrix modified with flux at different process parameters.

Sample	Avg. Precipitate size (μm)	Volume fraction (%)
M80/5	0.46 ± 0.2	8
M140/5	0.87 ± 0.3	5.3
M200/5	1.11 ± 0.3	2.1

Accepted for publication in *Surface and Coatings Technology*, Vol. 405, 126533, 2021, doi: https://doi.org/10.1016/j.surfcoat.2020.126533

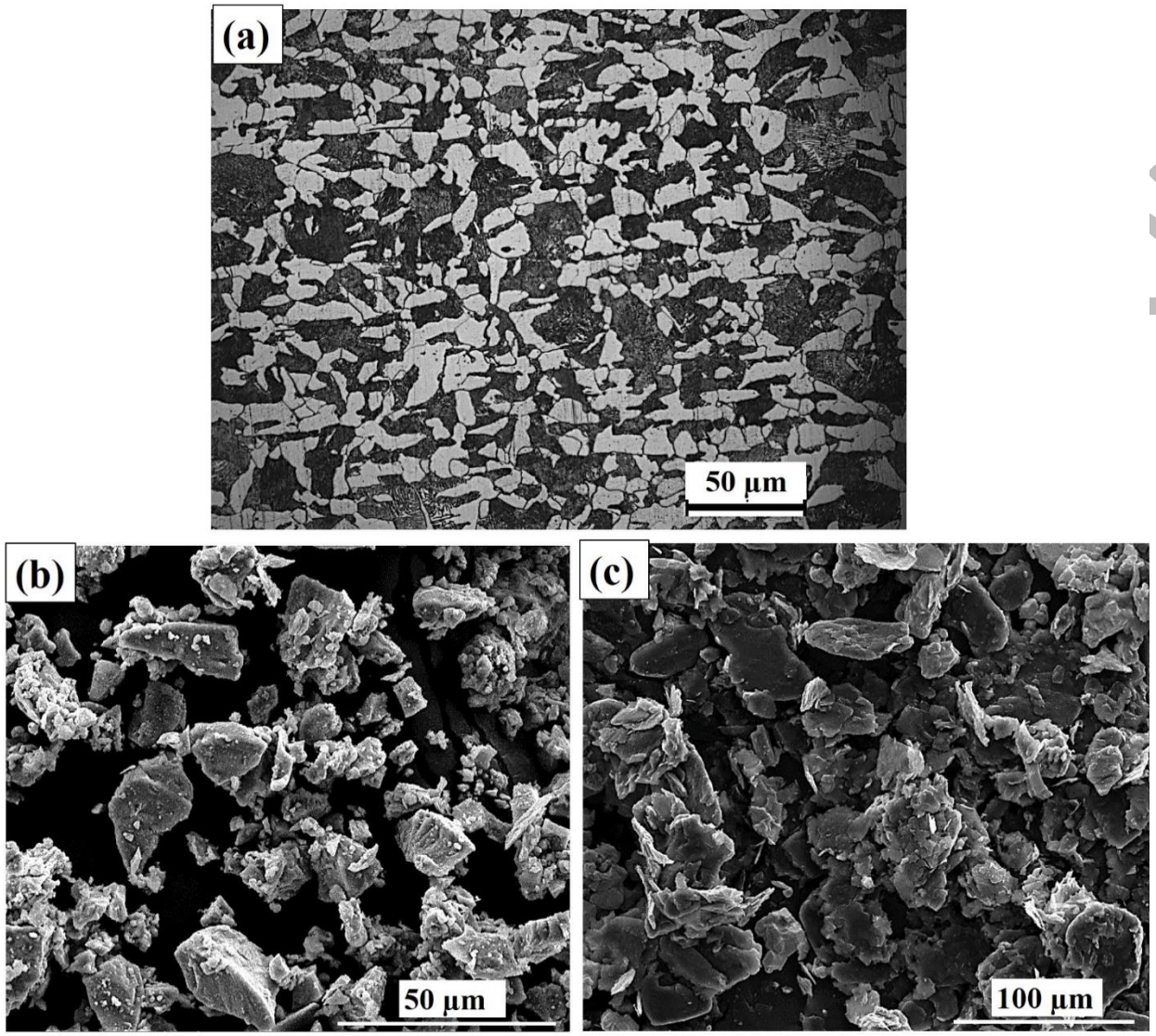

Fig. 1 (a) Microstructure of 8620 steel base metal. Morphology of the precursor powders (b) Titanium (c) Graphite.

Accepted for publication in *Surface and Coatings Technology*, Vol. 405, 126533, 2021, doi: https://doi.org/10.1016/j.surfcoat.2020.126533

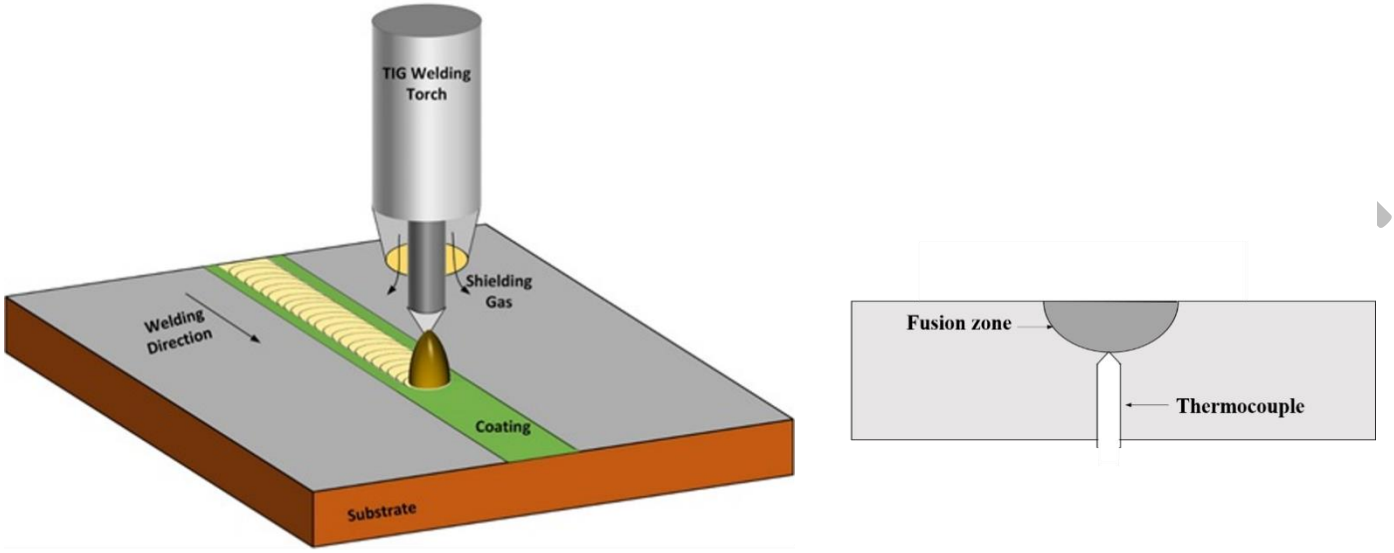

Fig. 2 Schematic diagram of (a) TIG arc surfacing of the substrate with preplaced flux coating and (b) placement of the thermocouple at the fusion zone.

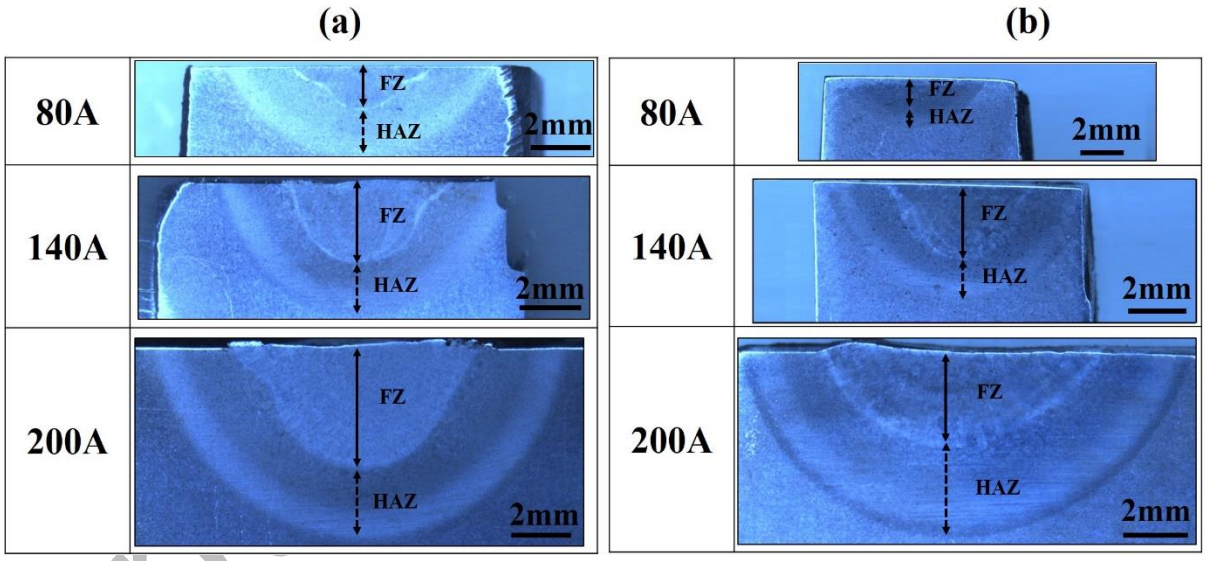

Fig. 3 Effect of arcing current on the geometry of fusion zone at a given arcing speed of 5 cm/min in case of arcing (a) with and (b) without flux.

Accepted for publication in *Surface and Coatings Technology*, Vol. 405, 126533, 2021, doi: https://doi.org/10.1016/j.surfcoat.2020.126533

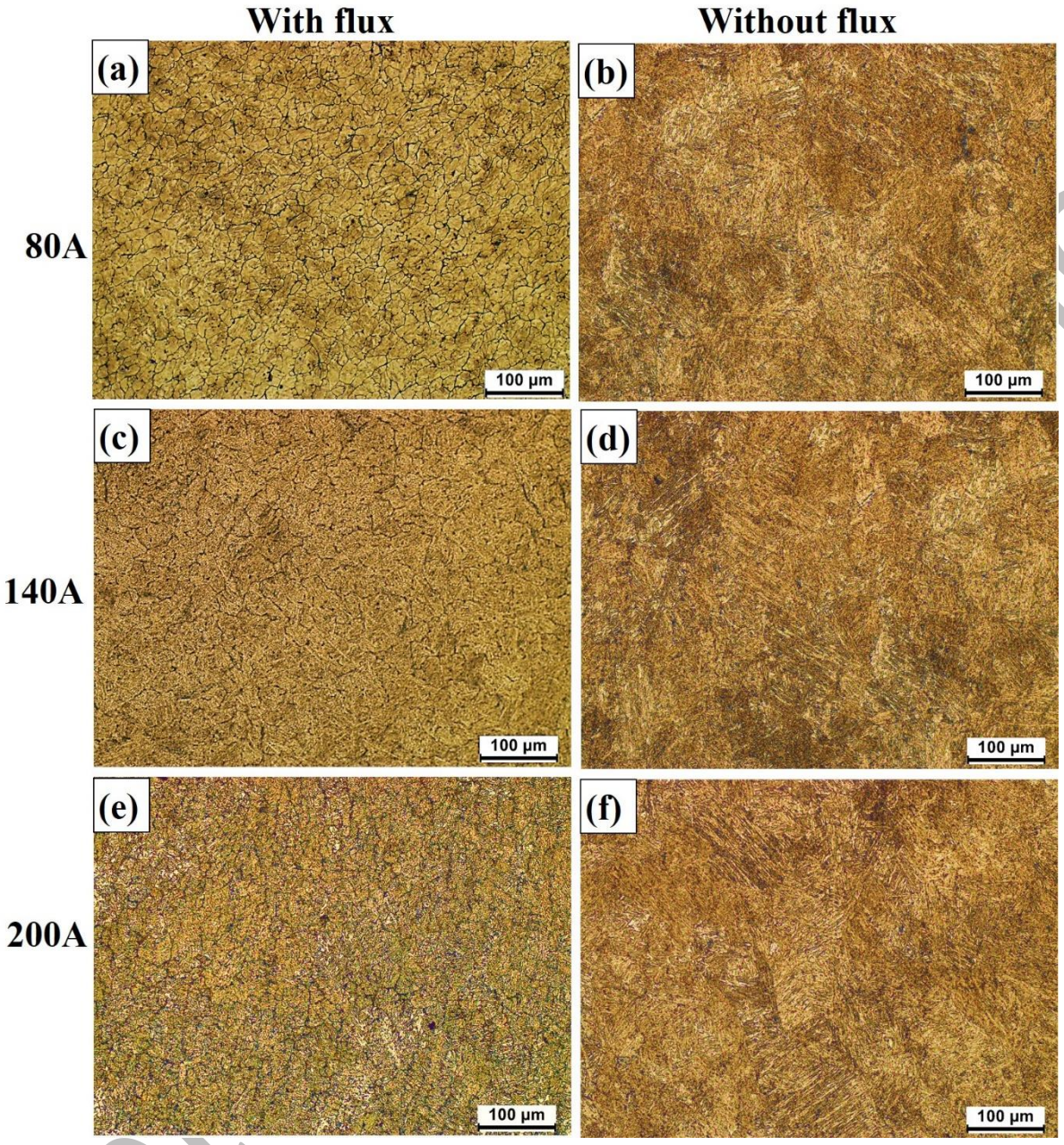

Fig. 4 Optical micrograph of the modified surface with flux at (a) 80A (c) 140A (e) 200A and without flux at (b) 80A (d) 140A (f) 200A

Accepted for publication in *Surface and Coatings Technology*, Vol. 405, 126533, 2021, doi: https://doi.org/10.1016/j.surfcoat.2020.126533

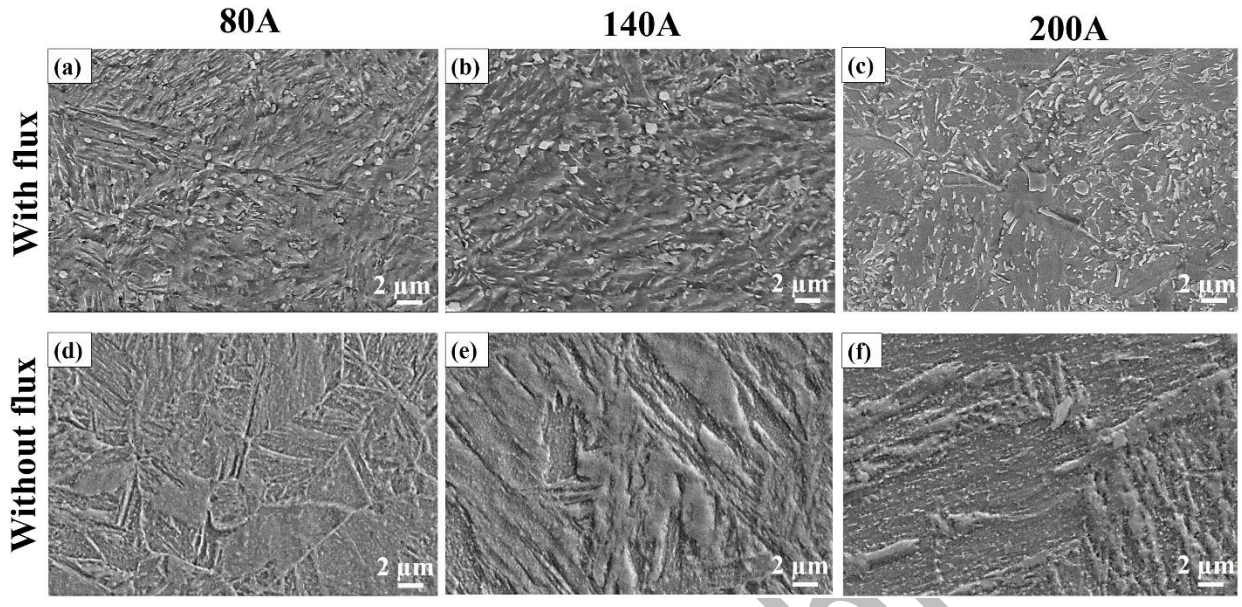

Fig. 5 FESEM images of the surface modified with flux (a)-(c) and without flux (d)-(f). (a,d) shows the modified surface at 80A, (b,e) at 140A and (c,f) at 200A

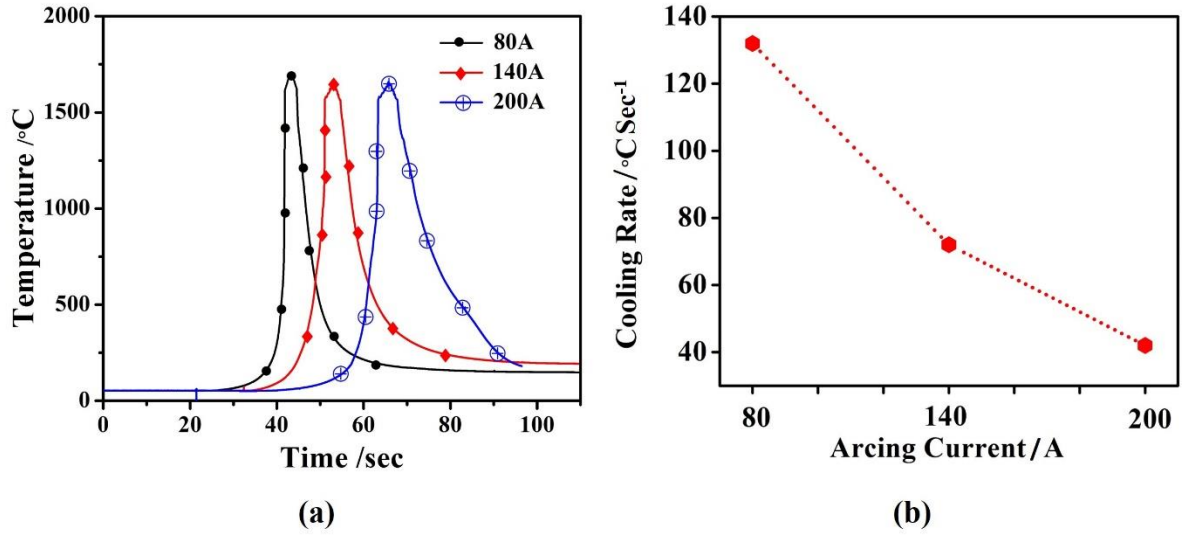

Fig. 6 Showing (a) thermal cycle plot of fusion zone of the modified surface with flux and (b) cooling rate within 800-500°C range (t_{8-5}) under variation of arcing current.

Accepted for publication in *Surface and Coatings Technology*, Vol. 405, 126533, 2021, doi: https://doi.org/10.1016/j.surfcoat.2020.126533

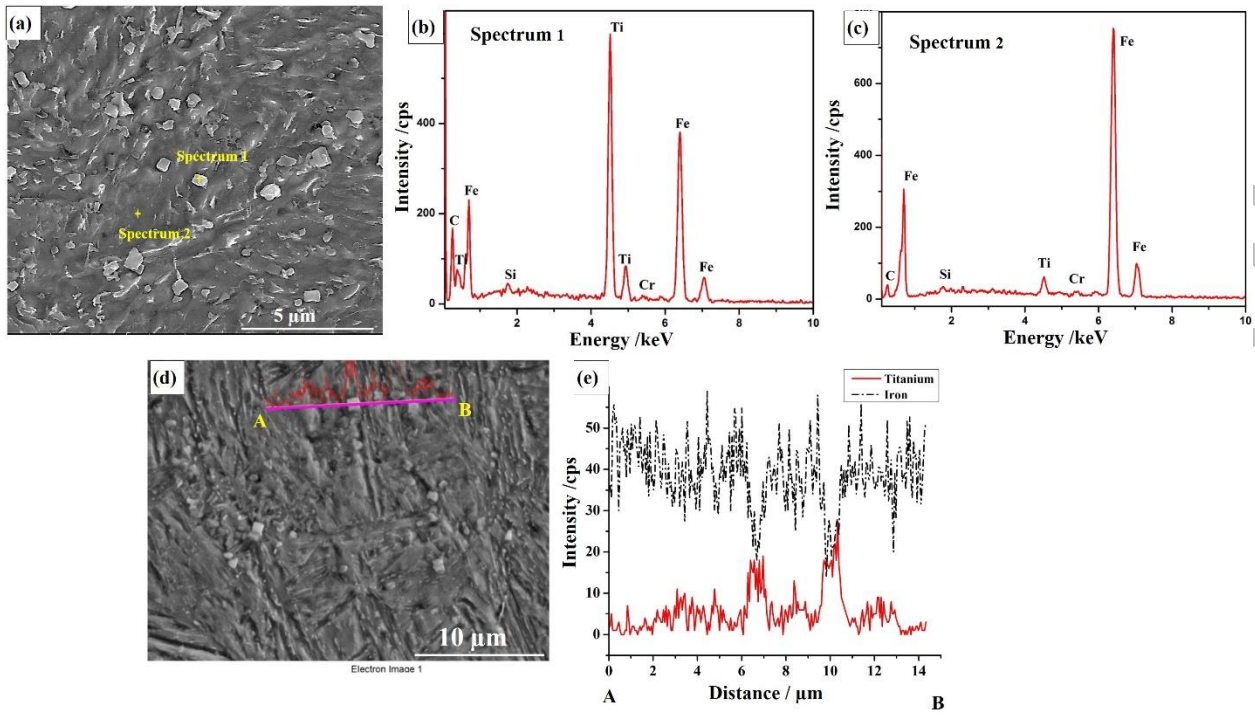

Fig. 7 EDS analysis of the modified zone prepared at arcing current of 80A with flux. (a) FESEM image of the in-situ grown particle reinforced matrix and corresponding (b) EDS point analysis on a particle and (c) EDS analysis of the matrix (d) EDS line scan of the modified matrix crossing a reinforced precipitate (e) EDS spectrum of the line AB

Accepted for publication in *Surface and Coatings Technology*, Vol. 405, 126533, 2021, doi: https://doi.org/10.1016/j.surfcoat.2020.126533

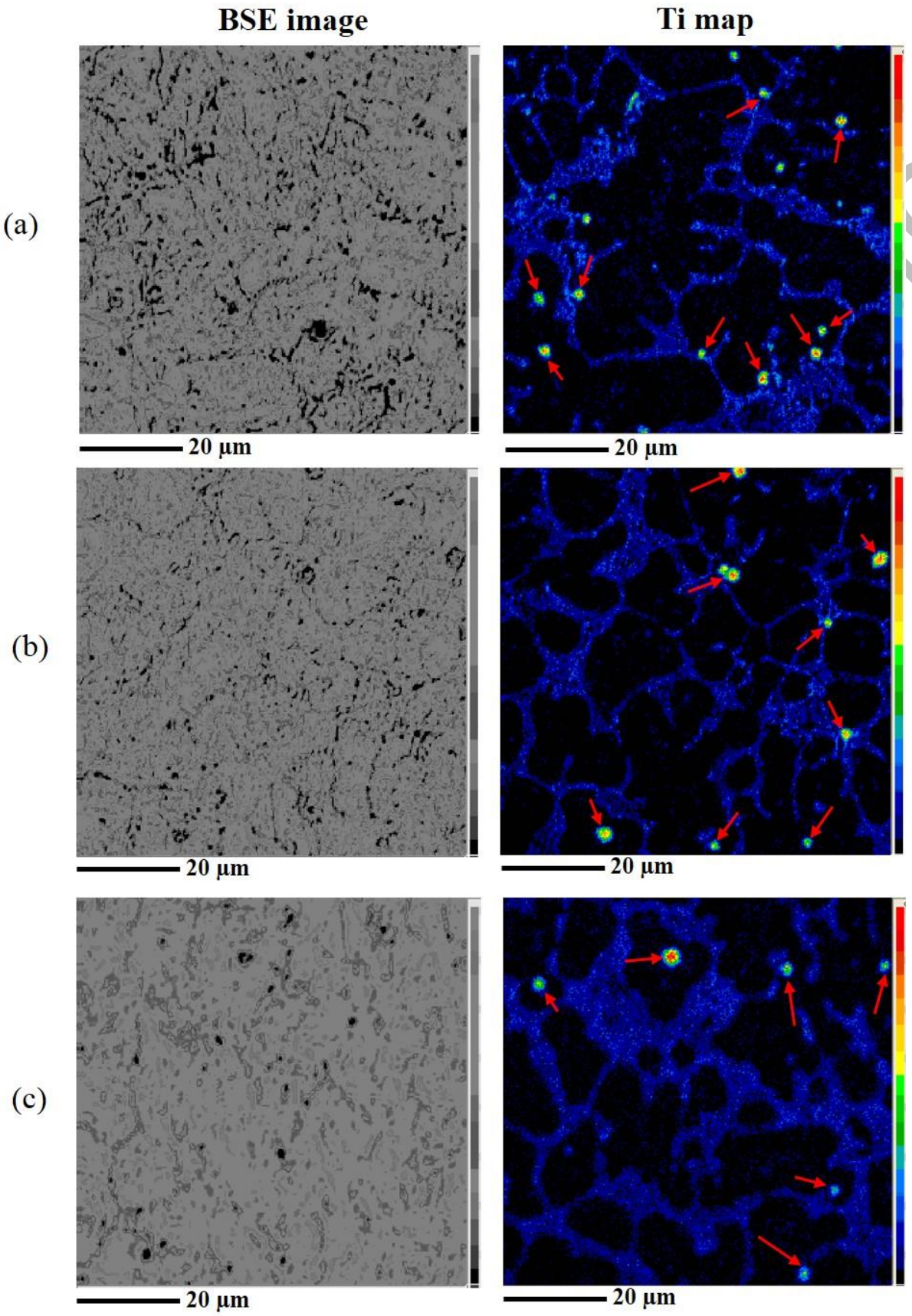

Fig. 8 Ti mapping (arrow marked) of *in-situ* grown TiC on modified surface with flux prepared at arcing current of (a) 80A, (b) 140A and (c) 200A.

Accepted for publication in *Surface and Coatings Technology*, Vol. 405, 126533, 2021, doi: https://doi.org/10.1016/j.surfcoat.2020.126533

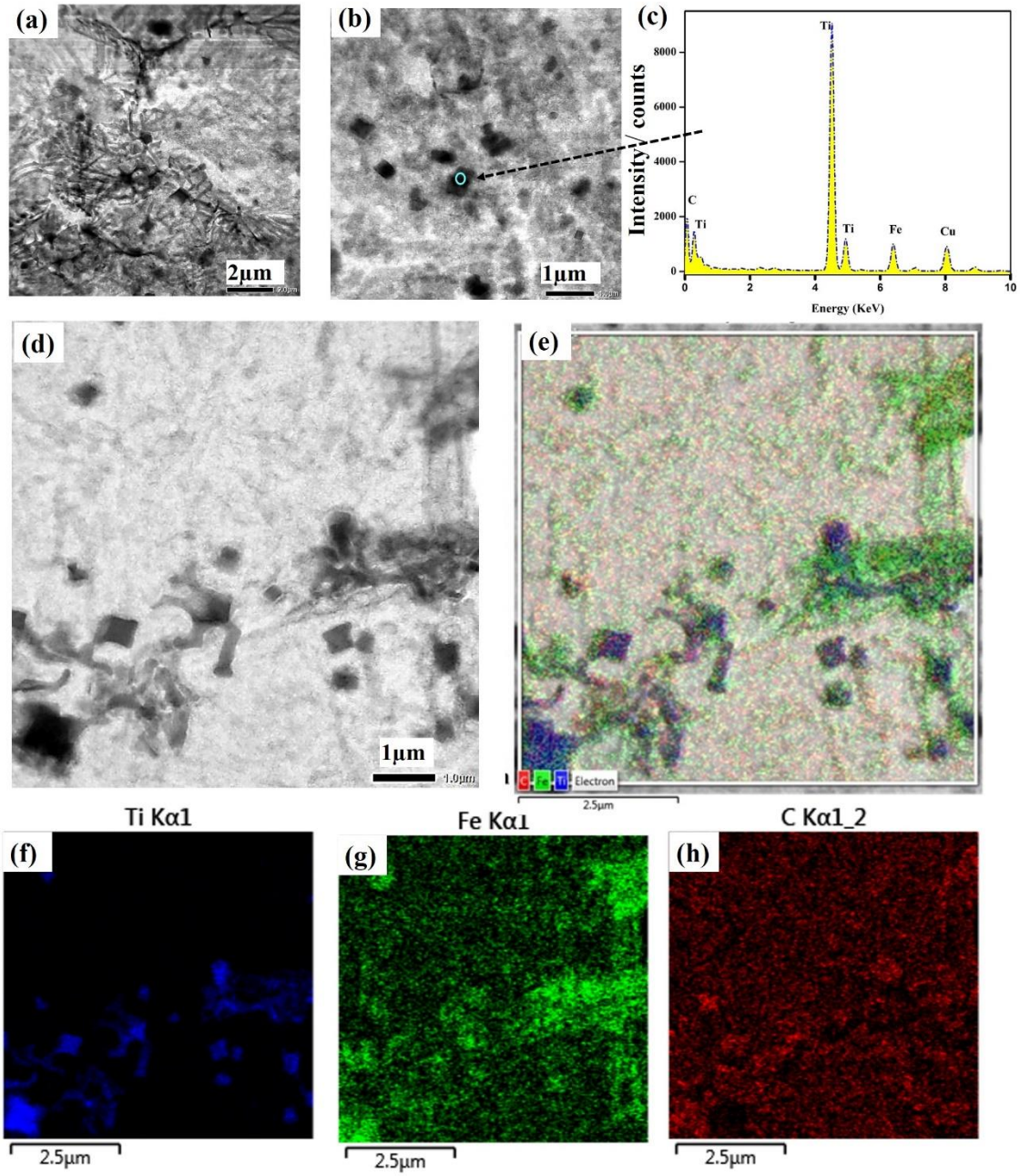

Fig. 9 STEM images of the extracted carbide layer from the modified surface with the addition of flux at 80A, (a) formation of the carbide on and at the vicinity of the grain boundary, (b)-(c) EDS analysis of the precipitate, (d) Mapping of the precipitate, (e) combined elemental mapping comprising Fe, Ti and C, (f) individual mapping of Ti, (g) individual mapping of Fe (h) individual mapping of C.

Accepted for publication in *Surface and Coatings Technology*, Vol. 405, 126533, 2021, doi: https://doi.org/10.1016/j.surfcoat.2020.126533

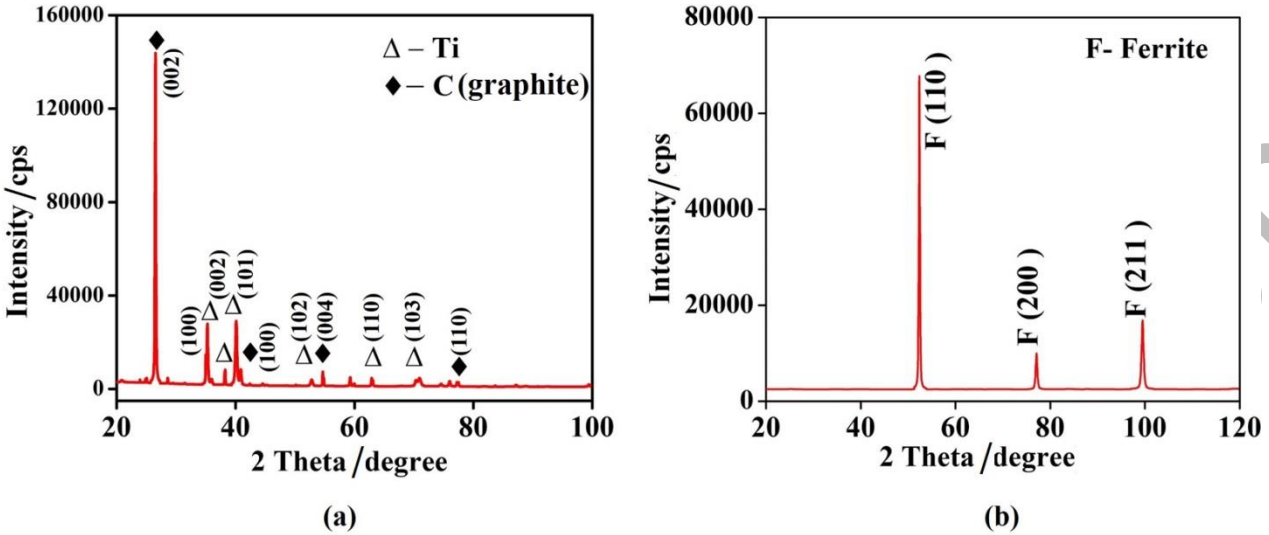

745
746
747 **Fig. 10** XRD pattern of the (a) precursor powder mix and (b) base material.
748

Accepted for publication in *Surface and Coatings Technology*, Vol. 405, 126533, 2021, doi: https://doi.org/10.1016/j.surfcoat.2020.126533

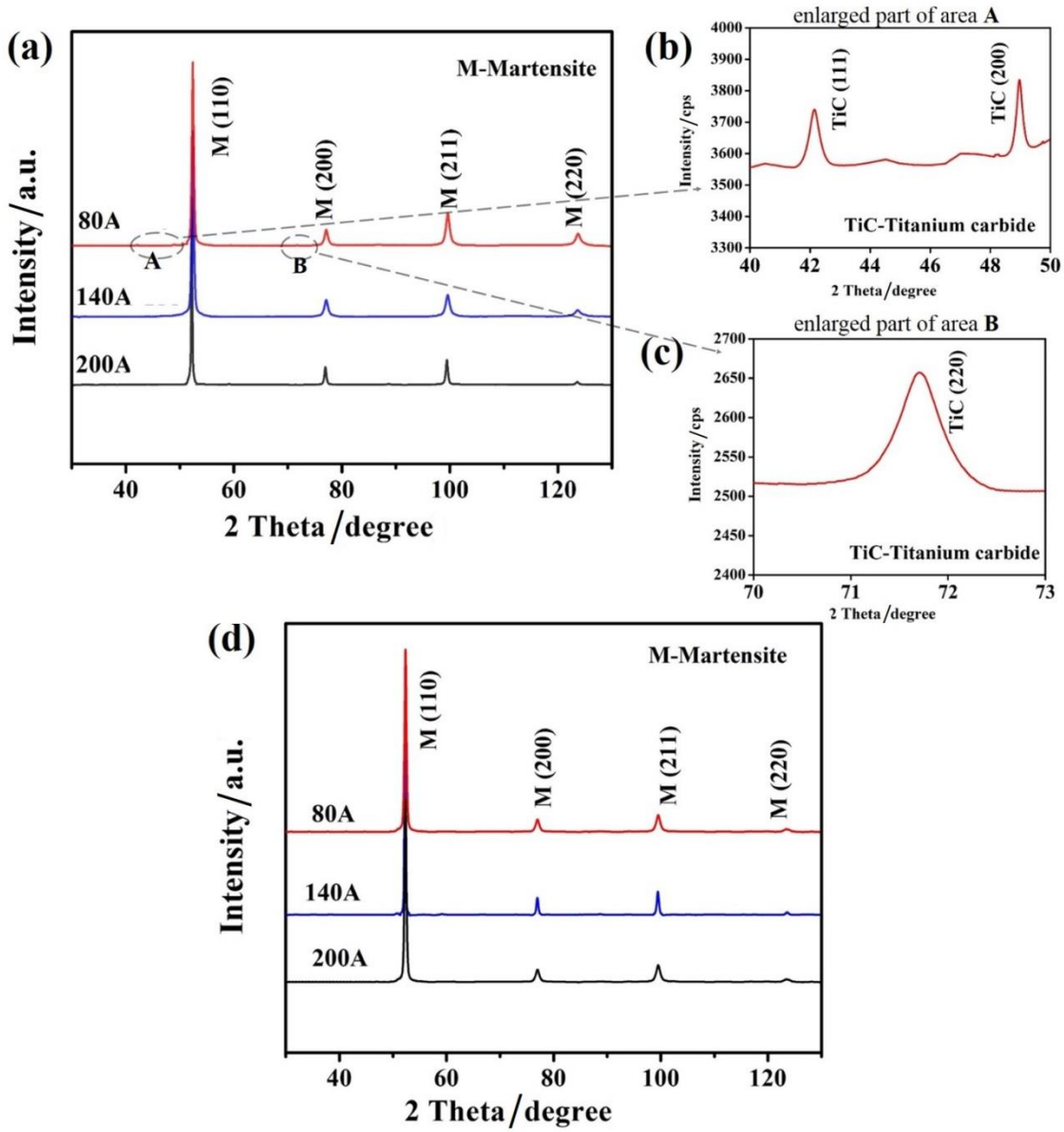

Fig.11 (a) XRD plots of the modified surface with flux at different processing parameter of 80, 140 and 200A, (b) enlarged view of area A showing titanium carbide peak (c) enlarged view of area B, (d) XRD plots of surface modified without flux at 80, 140 and 200A.

Accepted for publication in *Surface and Coatings Technology*, Vol. 405, 126533, 2021, doi: https://doi.org/10.1016/j.surfcoat.2020.126533

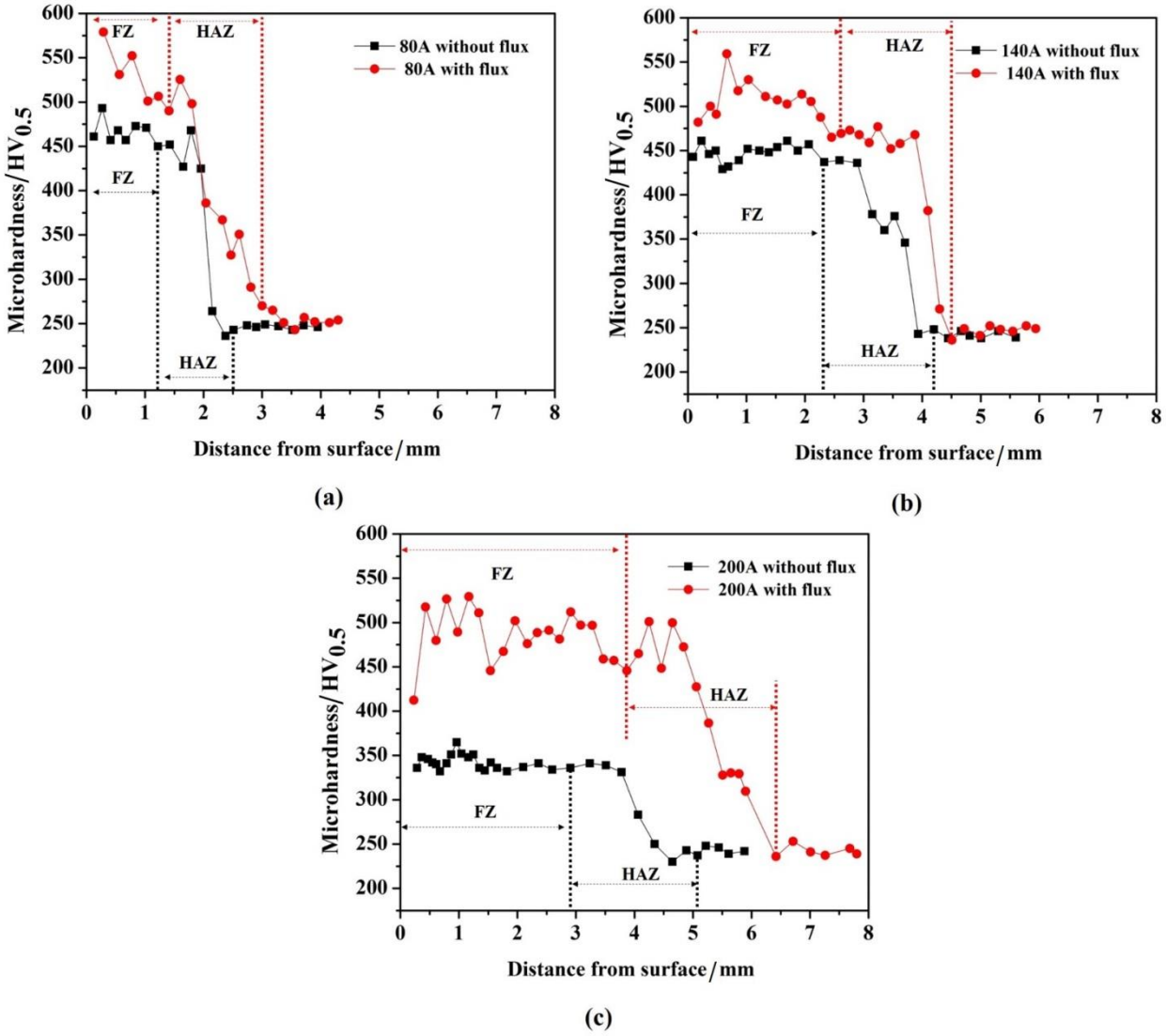

Fig.12 Microhardness distribution across the depth from top surface of the FZ to the base metal of the modified surface prepared with and without flux at the arcing currents of (a) 80A, (b) 140A (c) 200A.

Accepted for publication in *Surface and Coatings Technology*, Vol. 405, 126533, 2021, doi: https://doi.org/10.1016/j.surfcoat.2020.126533

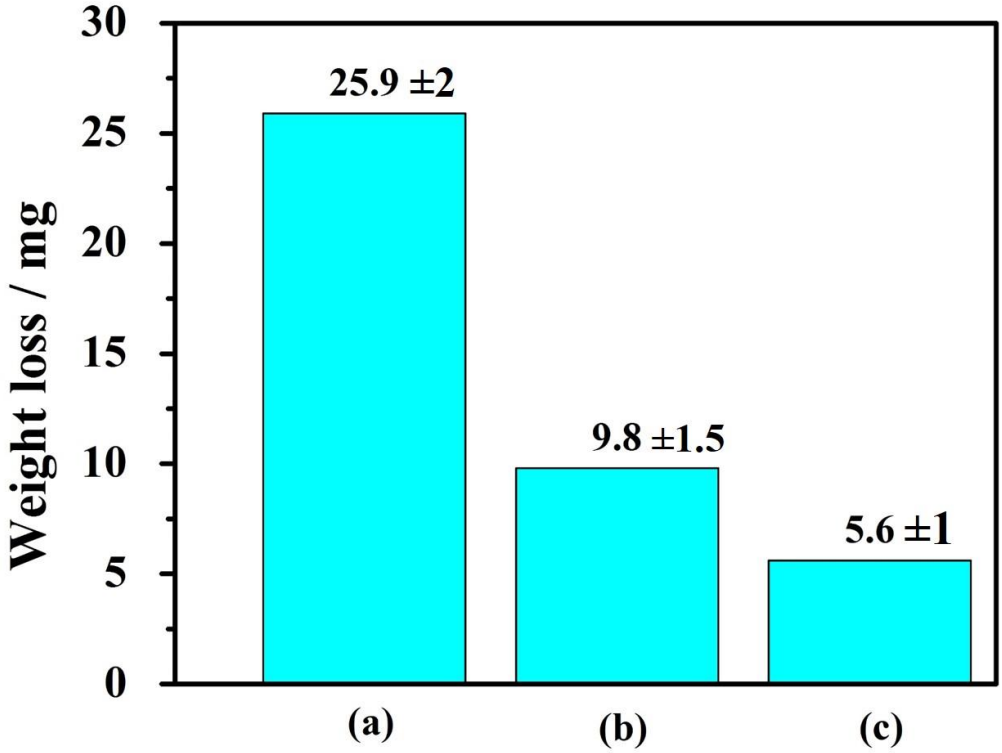

Fig. 13 Weight loss of various surface under dry sliding wear test of duration of 60 min of (a) 8620 steel substrate in as received condition, (b) modified without flux at 80A, (c) modified with flux at 80 A.

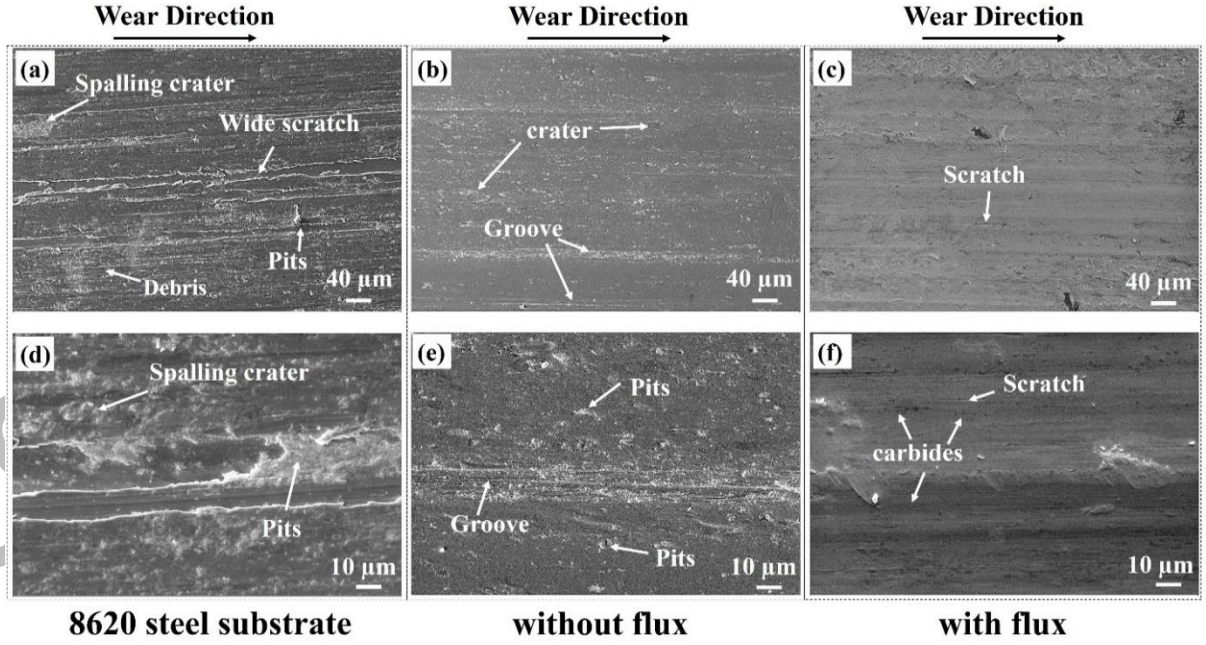

Fig. 14 FESEM image of the surface at two different magnifications after wear test (a), (d) 8620 steel substrate in as received condition (b), (e) modified surface without flux at 80A (c), (f) modified with flux at 80 A.